



A Simplified Model of Tethered Projectile Systems Wrapping Around Targets in Space and a Preliminary Capture Scheme Based Thereon

Hongzhi Ma^{1,2} · Ding Lan^{1,2} · Tao Wang³ · Fude Wang⁴

Received: 28 October 2022 / Accepted: 21 November 2022 / Published online: 8 December 2022
© The Author(s), under exclusive licence to Springer Nature B.V. 2022

Abstract

The Euler-Eytelwein equation indicates that the tension from one end of the rope to the other end decays exponentially with the wrapping angle after wrapping around a target object, and the tensions at two ends can differ by several orders of magnitude. The ability to scale the force magnitude of this wrapping structure may be exploited for space captures. This paper simplifies the modeling of the actual scene of space capture, analyzes the kinematic characteristics of the wrapping process of tethered projectile systems, and obtains the trajectory equation of the projectile. Carrying out the force analysis of the element, forces acting on the satellite and the target object under different friction coefficients are obtained. Finally, considering two constraints of rope tension and wrapping time, as well as the number of wrapping turns for safe, a design scheme of projectile velocity and initial rope length required for successful capture is proposed.

Keywords Space capture · Tethered projectile systems · Wrapping · Force analysis

Introduction

In space, debris removal, satellite maintenance (Inaba et al. 2006), spacecraft docking and planetary exploration are important needs in space engineering. A variety of capture schemes in space can be used to meet these needs.

Contact capture schemes in space are divided into two types (Shan et al. 2016): stiff captures and flexible captures. Stiff captures, such as tentacles capturing, single robotic arm capturing, multiple robotic arms capturing (Xu et al. 2019) and mechanical effectors, are already used in on-orbit servicing missions. Flexible captures have advantages of large

capture range, small impact force when capturing and saving storage space after folded. Most of flexible captures, such as net capturing (Xu et al. 2020), tether–grripper mechanism, harpoon mechanism, etc., stay in the conceptual design stage. RemoveDebris mission (Aglietti et al. 2020; Forshaw et al. 2020) funded by European Commission is the world's first Active Debris Removal (ADR) mission. Its mission flow includes conceptual design–manufacture, assembly integration and testing of payloads–launch–operations in orbit. And it successfully demonstrated technologies of net capture and harpoon capture in orbit in 2018.

In addition, there are some recent researches in captures in space. References (Liu et al. 2014; Pan et al. 2020) studied a rope end mechanism of space manipulator through simulation, and compared various strategies for space capture using three wire ropes to wrap a target together. Based on origami principle, reference (Sun et al. 2019) designed an adaptive capture mechanism that can be unfolded to form different grasping configurations according to different sizes of space debris.

One can see that most of the mechanisms of flexible captures belong to tether systems. Concepts of the Active Tether System (AST) for planetary exploration were systematically modeled by the reference (Quadrelli et al. 2017), in which tether dynamics, end effector dynamics, contact interactions, and tether materials were described, and three scenarios were considered: a tether made of switchable materials, a

✉ Ding Lan
landing@imech.ac.cn

✉ Tao Wang
wangt@microsatte.com

¹ Key Laboratory of Microgravity (National Microgravity Laboratory), Institute of Mechanics, Chinese Academy of Sciences, Beijing 100190, China

² School of Engineering Science, University of Chinese Academy of Sciences, Beijing 100049, China

³ Innovation Academy for Microsatellites of Chinese Academy of Sciences, Shanghai 201203, China

⁴ Wide range Flight Engineering Science and Applications Center, Institute of Mechanics, Chinese Academy of Sciences, Beijing 100190, China

tether for close operation and a tether connected to small objects for rendezvous/landing. Inspired by the reference (Quadrelli et al. 2017), this paper studies in detail the process of a tether-projectile system wrapping targets in space and the preliminary capture scheme based on wrapping.

Many researches have been done on the wrapping dynamics of tethered projectile systems on the ground. A Hyper-Flexible Manipulator (HFM) is made up of one-dimensional ultra-flexible elements that are highly deformable cable-like elements such as wires, tethers, ropes, and whips. The reference (Suzuki et al. 2005) divides the casting and winding manipulation with HFM into four stages: casting, contacting, winding and holding. And the HFM was modeled using a multi-link system connected by inelastic joints, and casting methods such as sinusoidal actuation and sudden halt were simulated. The reference (Suzuki et al. 2006) studied the casting method of single swing actuation used by HFM for wrapping through experiments and simulations. Compared with traditional parameter-recognized, feed-forward controlled casting operations, the reference (Ito et al. 2017) experimentally studied a casting operation based on high-speed visual feedback control, which can generate a suitable trajectory and achieve a robust winding. In references (Hill et al. 2015; Hill 2018), a tethered projectile was formed from an end-weighted cable, and the rebound ability of the tethered projectile is used to successfully wind targets in experiments and simulations.

However, as far as we know according to the literature research, there are little researches on wrapping using tethered projectile systems in space. The reference (Quadrelli et al. 2017) briefly mentions the problem of wrapping targets by a tether in space in the form of an simulation example, but does not analyze it in detail in the aspects of movement and force.

The research in this paper includes the analysis of kinematic behaviors of tethered projectile systems wrapping in space (Chapters 2 and 3), the force analysis (Chapter 4), and designs of preliminary capture based thereon (Chapter 5). The so-called initial capture means that the capture scheme we designed is the first step in a complete capture. The use of tethered projectile systems to establish connections between spacecrafts and targets is conducive to the smooth progress of subsequent tasks, such as momentum exchange to eliminate the relative velocity, closing the distance, rendezvous and dock, drag and remove debris out of orbit.

Kinematic Analysis

In practical engineering, if target objects are cooperative, the cross-sections of them can be designed to required regular shapes. But shapes of non-cooperative target objects may be arbitrary. For the convenience of theoretical analysis, we

simplify the target object to a cylinder here, first studying the case of a circular cross-section, and then expanding it to the case of a regular N-sided cross-section.

The target and satellite considered in this paper are assumed to be massive objects, so the effect of ropes on the motion of satellites and targets can be ignored during the wrapping process. In this chapter and the 3th chapter, it is assumed that positions of the satellite and target are fixed. Here, the cylindrical capture target can be considered as a bulge on a massive object.

The research in this paper is limited to the above two conditions, while applications of this paper can be very wide, which lays the foundation for researches of more complex situations in the future.

Target Objects with Circular Cross-Section

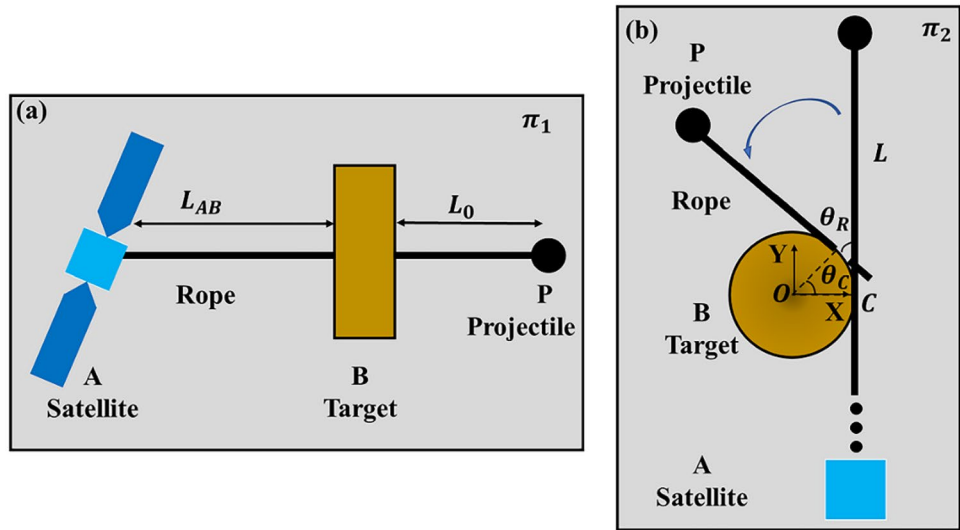
The trajectory of projectile during a wrapping process is analysed here. As shown in Fig. 1a, a satellite A throws a tethered projectile system to wrap around and capture a target object B in space. The initial length of rope for wrapping is L_0 , and the distance between A and B is L_{AB} . As shown in Fig. 1b, assuming that the target object is a cylinder with a radius r_B , a length L_B , and the center of circle at point O. The contact point between the rope and the cylinder is C, and the length of wrapping rope is L . A coordinate system OXY is established to be stationary relative to the satellite, the origin is at point O, and the X-axis points to C at the initial contact. When wrapping, the angular displacement of point C around point O, that is, the angle between OC and X-axis, is θ_C . The corresponding angular velocity is ω . The angle between rope CP and X-axis is θ_R . The lateral dimension of rope is ignored as it is much smaller than the target object's radius.

The motion of projectile is decomposed first. In this problem, the "Wrapping spiral motion" (WSM) of projectile P in the coordinate system OXY can be decomposed into two motions, namely the Archimedean spiral motion (ASM) (Heath 1921) and translational motion along a circle. As shown in Fig. 2a, a coordinate system CX_1Y_1 is established, where $X_1 \parallel X$, $Y_1 \parallel Y$. The motion of projectile P in the coordinate system CX_1Y_1 is ASM, and the trajectory equation is

$$\begin{cases} x_1 = \left(L_0 - r_B \int_0^t \omega dt \right) \cos \left(\int_0^t \omega dt + \frac{\pi}{2} \right) \\ y_1 = \left(L_0 - r_B \int_0^t \omega dt \right) \sin \left(\int_0^t \omega dt + \frac{\pi}{2} \right) \end{cases},$$

of which the expression in polar coordinates (ρ_1, θ_1) is $\rho_1 = (L_0 + \pi r_B / 2) - r_B \theta_1$. The coordinate system CX_1Y_1 performs translational motion as a whole along with point C and along the contour of the target B. The trajectory equation of point C is

Fig. 1 Schematic diagram of a satellite using the wrapping of a tethered projectile system to capture a target object. **a** The plane π_1 determined by the satellite A, the target objects B and the longitudinal directions of B; **b** the plane π_2 determined by the satellite A, the target objects B and the cross-section of B



$$\begin{cases} x = r_B \cos\left(\int_0^t \omega dt\right) \\ y = r_B \sin\left(\int_0^t \omega dt\right) \end{cases}$$

In the coordinate system CX_1Y_1 , ASM can also be decomposed into two motions, namely linear motion and rotational motion. A coordinate system CX_2Y_2 is established as shown in Fig. 2b, where $X_2 \parallel CP$, $Y_2 \perp CP$. The motion of projectile P in the coordinate system CX_2Y_2 is a linear motion, of which the motion equation is

$$\begin{cases} v_{\rho 1} = -\omega(t)r_B \\ L = L_0 - r_B \int_0^t \omega(t)dt \end{cases}$$

At the same time, the coordinate system CX_2Y_2 rotates around point C as a whole with an angular velocity of ω .

Then, superimpose the decomposed motions in turn. As shown in Fig. 2b, the velocity of ASM of projectile P in the coordinate system CX_1Y_1 is

$$\begin{cases} v_{\rho 1} = -\omega(t)r_B \\ v_{\theta 1} = \omega(t)\left(L_0 - r_B \int_0^t \omega(t)dt\right) \end{cases}$$

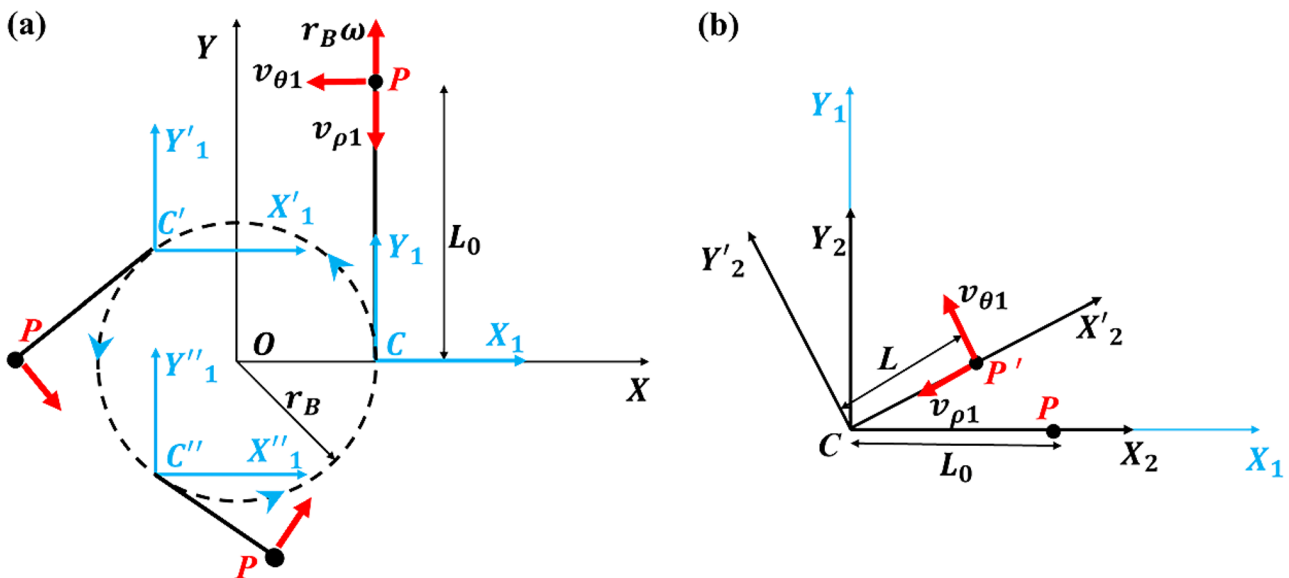


Fig. 2 Decomposition and superposition of WSM. **a** In coordinate system OXY , ASM and translational motion of coordinate system CX_1Y_1 are superimposed to form WSM; **b** in coordinate system

CX_1Y_1 , linear motion of projectile and circular motion of coordinate system CX_2Y_2 are superimposed to form ASM

As shown in Fig. 2a, the projectile superimposes a velocity $v\omega(t)$ along the direction of \overline{CP} in the coordinate system OXY, because the coordinate system CX_1Y_1 as a whole performs a translational motion along the circumference around point O with angular velocity $\omega(t)$. The velocity of projectile in the coordinate system OXY is

$$\begin{cases} v_\rho = v_{\rho 1} + r_B\omega(t) = 0 \\ v_\theta = v_{\theta 1} = \omega(t)\left(L_0 - r_B \int_0^t \omega(t)dt\right) \end{cases}.$$

As a summary, the following three features of WSM is obtained:

1. WSM is a compound motion obtained by superimposing three simple motions twice.
2. In WSM, the projectile has only a tangential velocity \overline{v}_θ perpendicular to rope CP, and no normal velocity \overline{v}_ρ parallel to rope. Therefore, on the trajectory of WSM, the tangent at any point is perpendicular to rope, and the normal is parallel to rope and tangent to the cylinder.
3. The projectile is not subject to external forces other than the tension of rope. The tension satisfies $\overline{T} \perp \overline{v}_\theta$, so the magnitude of velocity v_θ remains unchanged during wrapping, which is

$$v_\theta = \omega_1(L_{AB} + L_0) = v \tag{1}$$

Next, the trajectory equation of projectile P is solved. When the rope is just in contact with the target, the angular velocity of rope rotation is $\omega_0 = v/L_0$. During the wrapping process, the rope is always tangent to the cylinder, so the rotation angle and angular velocity of point C around point O are the same as that of the rotation of rope itself. The governing equations of the length of wrapping rope L are

$$\begin{cases} \frac{dL}{dt} = -r_B\omega \\ \omega = \frac{v}{L} \\ L(t=0) = L_0 \end{cases}.$$

Solving this differential equation yields the rope length as

$$L = L_0\tilde{L}, \tag{2}$$

where, $\tilde{L} = (1 - t/t_{end})^{0.5}$.

From $L=0$, the end time of wrapping is obtained as

$$t_{end} = \frac{L_0^2}{2vr_B}. \tag{3}$$

And the angular velocity is

$$\omega = \omega_0\tilde{L}^{-1}.$$

As shown in Fig. 3, the rope length L gradually decreases until it reaches 0 and the angular velocity ω becomes faster and faster as the wrapping progresses.

The rotation angle of point C around point O is

$$\theta_C = \int_0^t \omega dt = \frac{1}{\mu_c} (1 - \tilde{L}), \tag{4}$$

where $\mu_c = r_B/L_0$ whose physical meaning will be given later. The angle between rope and X-axis is $\theta_R = \theta_C + \pi/2$. Therefore, the parametric equation of trajectory of point C and trajectory of projectile are

$$\begin{cases} x = r_B \cos \theta_C \\ y = r_B \sin \theta_C \end{cases},$$

and

$$\begin{cases} x = r_B \cos \theta_C + L \cos \theta_R \\ y = r_B \sin \theta_C + L \sin \theta_R \end{cases},$$

respectively. Define the number of wrapping turns as

$$n = \frac{L_0}{2\pi r_B}, \tag{5}$$

then trajectories of WSM of projectile with numbers of wrapping turns (a) $n=1$, (b) $n=2$ and (c) $n=4$ are shown in Fig. 4.

Target Objects with Regular N-sided Cross-Section

More generally, consider target objects with regular N -sided cross-section. Figure 5 presents schematic diagrams of wrapping with (a) a regular triangle, (b) a regular pentagon and (c) a regular heptagon in cross-section. Consider an inscribed regular N -gon ($N \geq 3$) of a circle with radius r_B , then its side length is $f_N = 2r_B \sin(\pi/N)$. Each time the rope wraps around a side, the angle swept by projectile in one arc

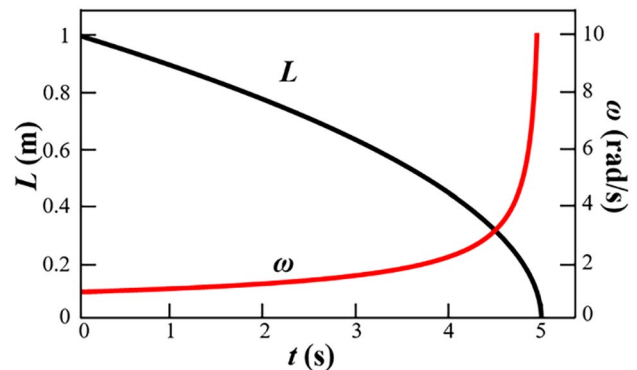


Fig. 3 Variation of the wrapping rope length L and the rotational angular velocity ω with time. $r_B = 0.1$ m, $v = 1$ m/s, $L_0 = 1$ m

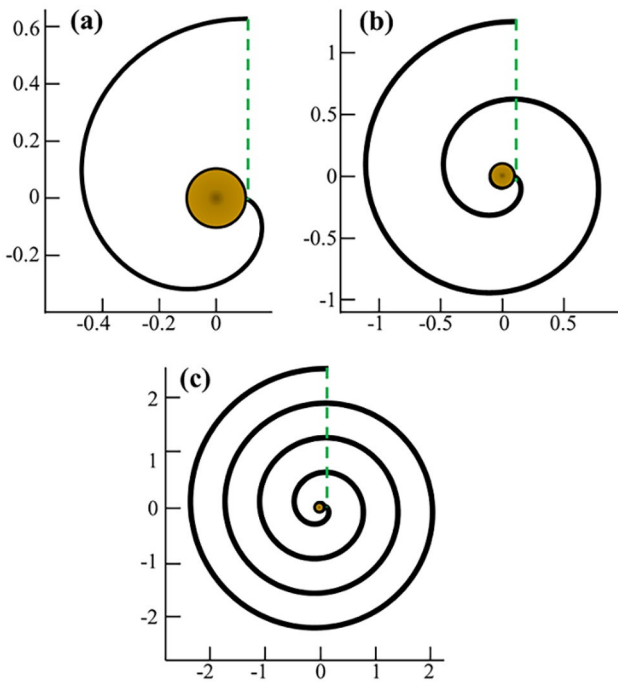


Fig. 4 Trajectories of the projectile's WSM. The number of wrapping turns and the initial rope length are (a) $n=1$, $L_0 = 0.6283$ m, (b) $n=2$, $L_0 = 1.2566$ m, and (c) $n=4$, $L_0 = 2.5132$ m, respectively. $r_B = 0.1$ m, $v = 1$ m/s

movement is $\theta_N = 2\pi/N$. Therefore, the time for projectile to complete the m -th arc movement is

$$t_m = \frac{\theta_N}{\omega_m} = \frac{\theta_N [L_0 - (m-1)f_N]}{v}$$

The cumulative wrapping time for the projectile to complete m arc motions is

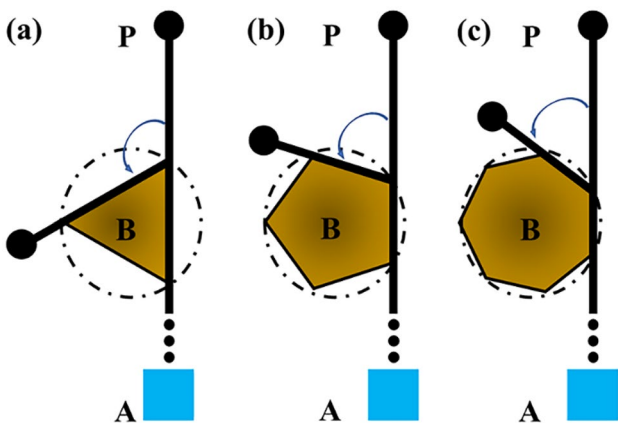


Fig. 5 Schematic of the wrapping a target object with regular N -sided cross-section. The numbers of sides are (a) $N=3$, (b) $N=5$, (c) $N=7$, respectively

$$t_{mEnd} = \sum_1^m t_m = \frac{\theta_N}{v} \left[mL_0 - m(m-1)\frac{f_N}{2} \right].$$

Assuming that the wrapping ends in the m -th arc motion, the rotation radius $R_m = L_0 - (m-1)f_N$ satisfies

$$0 < R_m \leq f_N$$

resulting in the range of the number of arcs m as

$$\frac{L_0}{f_N} \leq m < \frac{L_0}{f_N} + 1.$$

And m is an integer, so $m = \lceil L_0/f_N \rceil$, where $\lceil \cdot \rceil$ is a symbol of round up, that is, m is the smallest integer greater than or equal to L_0/f_N . Therefore, the cumulative wrapping time is

$$t_{mEnd} = \frac{2\pi}{Nv} \left(\left\lceil \frac{L_0}{2r_B \sin(\frac{\pi}{N})} \right\rceil L_0 - \left[\frac{L_0}{2r_B \sin(\frac{\pi}{N})} \right] \left(\left\lceil \frac{L_0}{2r_B \sin(\frac{\pi}{N})} \right\rceil - 1 \right) r_B \sin(\frac{\pi}{N}) \right).$$

The number of wrapping turns is $n \approx \frac{L_0 \theta_N}{f_N 2\pi} = \frac{L_0}{2Nr_B \sin(\frac{\pi}{N})}$.

Considering the limit case $N \rightarrow \infty$, then $\lim_{N \rightarrow \infty} \left[L_0 / (2r_B \sin(\frac{\pi}{N})) \right] = \infty$, so the rounding symbol $\lceil \cdot \rceil$ can be ignored. The following result

$$\lim_{N \rightarrow \infty} t_{mEnd} = \frac{\pi L_0^2}{2vr_B} \frac{1}{\lim_{N \rightarrow \infty} N \sin(\frac{\pi}{N})} = \frac{L_0^2}{2vr_B}$$

is obtained, which is consistent with the conclusion of the circular cross-section.

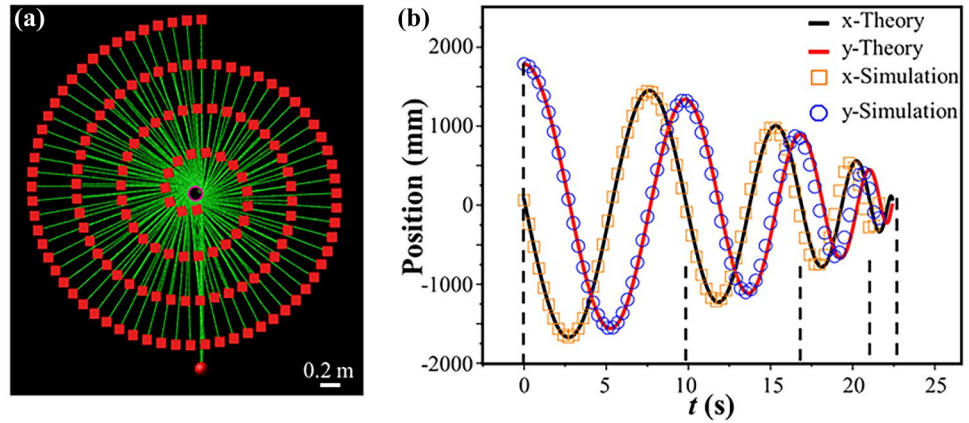
Each time the rope wrapping around a side of length f_N , the trajectory of projectile is an arc. When $N \rightarrow \infty$, $f_N \rightarrow ds = r_B d\theta_C$, and the regular polygon approaches to a circle. Therefore, in the process of rope wrapping around each micro-arc $r_B d\theta_C$ of the cylinder (the angle at which rope rotates is $d\theta_C$), the trajectory of projectile is also an arc. That is, the projectile performs circular motion at every instant, while the rotational radius and angular velocity of the circular motion keep changing with time as shown in Fig. 3.

Simulations

Method of Simulation

Simulations are performed using a method of Dynamics of Multi-body System (MSD), and the model is built as shown in Fig. 6. Projectile P is a box with the size of 100 mm*100 mm*200 mm, a density of $7.8 \cdot 10^3$ kg/m³, and an applied initial velocity v of 1 m/s horizontally pointing to the left (Fig. 6b). The target B is a pulley as shown in Fig. 6c, of which the position is fixed, the longitudinal lengths

Fig. 9 Simulation of $n = 4$. **a** Movement trajectory of which the time interval between two adjacent frames is 0.15 s. **b** The time-dependent displacements of projectile in x and y directions are compared with theoretical results. Vertical dashed lines represent the moments corresponding to integer numbers of turns. $L_0 = 1.7844$ m



Results of Simulation

Trajectory results of simulations with numbers of wrapping turns $n = 1, n = 2$ and $n = 4$ respectively are shown in Figs. 7a, 8a, 9a. As shown in Figs. 7b, 8b, 9b, contrasts between the displacements in the x and y directions of simulations and that of theory index and the theory indicate that simulation results are in good agreement with the results of theoretical analysis in Chapter 2.

Moreover, combining Eqs. (3) and (5), the relationship between the total time of wrapping and total number of turns is

$$t_{end} = \frac{2\pi^2 r_B}{v} n^2. \tag{6}$$

During the wrapping process, the time required to complete the n -th turn countdown to the end of wrapping is

$$t_{single} = t_{end}(n) - t_{end}(n - 1) = \frac{2\pi^2 r_B}{v} (2n - 1).$$

As shown in Fig. 10, the above two wrapping times form simulations are in good agreement with that of theory.

Force Analysis

In space, satellites and targets cannot be completely fixed like objects on the ground. Therefore, analyzing forces on satellites and targets during the rope wrapping process when satellites and targets are fixed is of important reference significance for considering the mechanical response of satellites and targets.

Force Analysis of Satellite

The force on satellite is analyzed first, which is equal to the tension of rope T_{holdt} between the target object and the satellite. The projectile performs circular motion at every instant, so the tension of rope between the target and the projectile is

$$T_{loadt} = \frac{m_p v^2}{L}, \tag{7}$$

where, m_p is the mass of projectile. During the wrapping process, the projectile is subjected to centrifugal force and tends to move away from the target radially. Therefore, the direction of movement trend of rope relative to the

Fig. 10 Comparison between simulation and theory: **a** the relationship between the total wrapping time t_{end} and the total number of turns n ; **b** the time required for the n -th last turn during the wrapping process

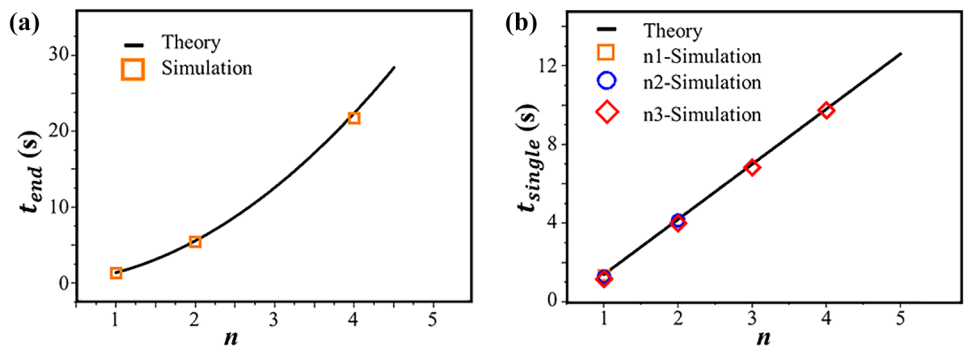
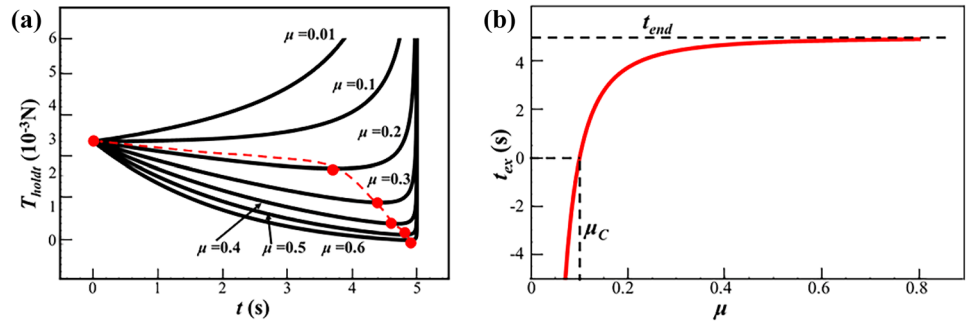


Fig. 11 **a** Variation of force acting on the satellite with time under different COFs. Red points represent positions of extremum time; **b** The change of extremum time t_{ex} with the COF μ . $r_B = 0.1$ m, $v = 1$ m/s, $L_0 = 1$ m, $m_p = 0.003$ kg, $\mu_c = 0.1$



target points towards the projectile. According to the Euler-Eytelwein equation (Shi et al. 2017), there have

$$T_{holdt} = T_{loadt} e^{-\mu\theta_c}, \tag{8}$$

Where, μ is the coefficient of friction (COF) between the rope and the target. Solving simultaneous Eqs. (2), (4), (7), (8), it is got as

$$T_{holdt} = T_0 \tilde{L}^{-1} \exp\left(-\frac{\mu}{\mu_c} (1 - \tilde{L})\right), \tag{9}$$

which is proportional to the tension $T_0 = m_p v^2 / L_0$ at the initial moment. From $d^2 T_{holdt} / dt^2 = 0$, the time corresponding to extreme value is obtained as

$$t_{ex} = t_{end} \left(1 - (\mu_c / \mu)^2\right).$$

The critical COF obtained from $t_{ex} = 0$ is

$$\mu_c = \frac{r_B}{L_0}$$

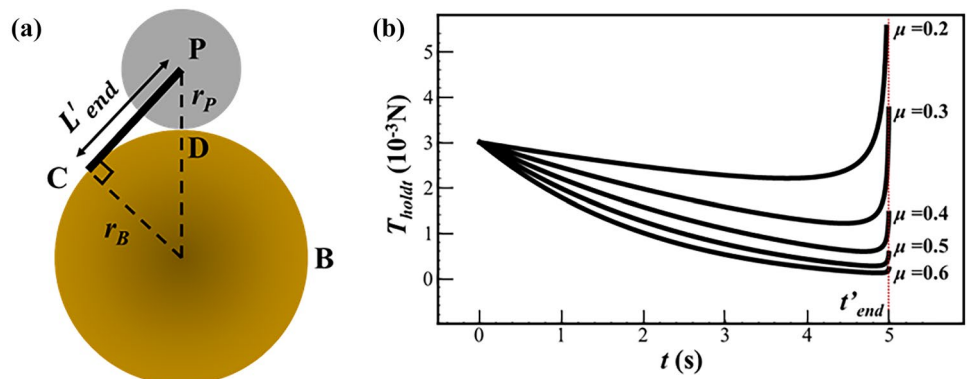
Combining the expression of extremum time t_{ex} and the characteristics of force–time curves as shown in Fig. 11a, it can be seen that in the range of $t \in (0, t_{end})$, the monotonicity of T_{holdt} is: when $\mu \leq \mu_c$, the extremum time is less than or equal to zero and T_{holdt} increases monotonically; when $\mu > \mu_c$, the extremum time is greater than zero, T_{holdt}

decreases first ($t \in (0, t_{ex})$) and then increases ($t \in (t_{ex}, t_{end})$). This feature of monotonicity in Eq. (9) is due to the competition between the exponential decay term determined by the Euler-Eytelwein equation and the increase term \tilde{L}^{-1} with singularity determined by the angular velocity ω . In practical applications, it is hoped that the smaller the force on satellite, the better. So, $\mu > \mu_c$ is required, and the larger the COF, the better. It can be seen from Fig. 11b that the extremum time t_{ex} increases with the increase of the COF, and gradually approaches t_{end} .

As shown in Fig. 11a, there are extreme points, after which the tension T_{holdt} increases rapidly due to the singularity of \tilde{L}^{-1} . However, as shown in Fig. 12a, in practical situations, three points of the center of projectile P, the contact point C between rope and the target and the contact point D between projectile and the target will not be overlapped, but to form a stable triangle ΔPCD . Therefore, the singularity as the length of rope equal to zero will not be reached. Assuming that the projectile is a sphere with a radius r_p . When the projectile is in contact with the target, rope will not be completely wrapped on the target, but a small section will be left, whose length is $L'_{end} = \sqrt{r_p^2 + 2r_B r_p}$. From Eq. (2), the actual end time corresponding to L'_{end} is

$$t'_{end} = t_{end} \left(1 - \frac{r_p^2 + 2r_B r_p}{L_0^2}\right).$$

Fig. 12 **a** The actual contact between the projectile P and the target B at the end of wrapping. **b** The force–time curves of satellite considering the actual end time $t'_{end} = 4.99$ s when $\mu > \mu_c$. $r_p = 0.01$ m, other parameter values are consistent with Fig. 11



As shown in Fig. 12b, when $\mu > \mu_c$, values of T_{holdt} at time t'_{end} are limited within a finite range and the values are small. Moreover, when μ is large (for example, the curve corresponding to $\mu = 0.6$), it can be approximated that T_{holdt} decreases monotonically in the range of $t \in (0, t'_{end})$.

In addition, when sizes of the projectile and the target are much smaller than the initial length of rope, there is $(r_p^2 + 2r_B r_p) / L_0^2 \ll 1$. So,

$$t'_{end} \approx t_{end}.$$

Force Analysis of Target Object

The force acting on the target is analyzed then. As shown in Fig. 13, force analysis of the rope element belong to the wrapping section is carried out as

$$\begin{cases} T \cos \frac{d\theta}{2} + dF_f = (T + dT) \cos \frac{d\theta}{2} \\ dF_N = T \sin \frac{d\theta}{2} + (T + dT) \sin \frac{d\theta}{2} \\ \mu dF_N = dF_f \end{cases}.$$

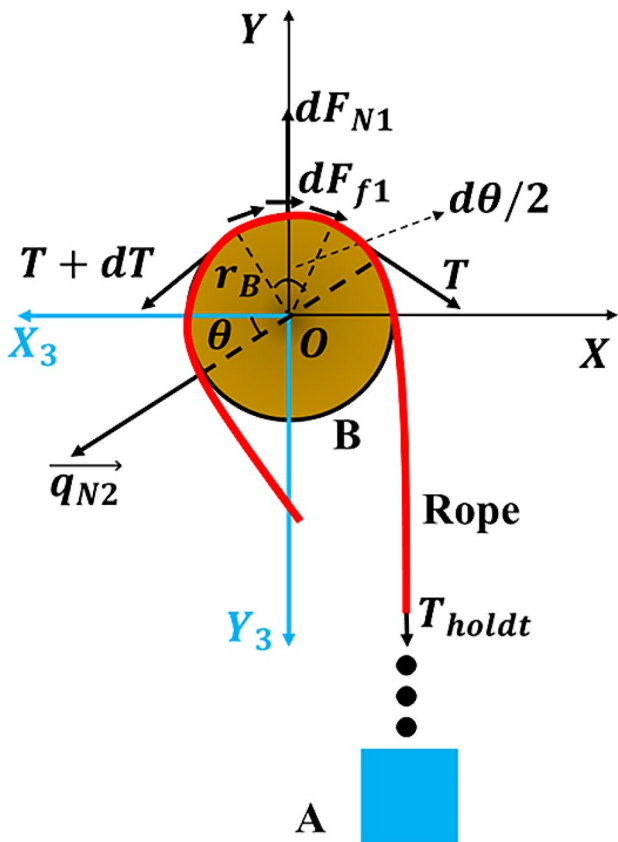


Fig. 13 Force analysis of the interaction between the rope and the target object

From $d\theta \approx 0$, $\cos(d\theta/2) \approx 1$, $\sin(d\theta/2) \approx d\theta/2$, the system of differential equations is simplified to

$$\begin{cases} dF_f = dT \\ dF_N = T d\theta \\ \mu dF_N = dF_f \end{cases}.$$

Solving the system of equations yields the supporting force of unit angle q_{N1} and the friction force of unit angle q_f as

$$\begin{cases} q_{N1} = \frac{dF_{N1}}{d\theta} = T = T_{holdt} e^{\mu\theta} \\ q_f = \frac{dF_f}{d\theta} \end{cases}.$$

According to Newton's third law of motion, the normal force of unit angle that rope acts on the target object is

$$\begin{cases} \overline{q_{N2}} = \frac{d\overline{F_{N2}}}{d\theta} = -\overline{q_{N1}} \\ q_{N2} = q_{N1} \\ 0 \leq \theta \leq \theta_C \end{cases}.$$

In the coordinate system Ox_3Y_3 shown in Fig. 13, perform the following vector decomposition of $\overline{q_{N2}}$

$$\begin{cases} \overline{q_{N2}} = (q_{N2x}, q_{N2y}) \\ q_{N2x} = q_{N2} \cos \theta \\ q_{N2y} = q_{N2} \sin \theta \end{cases}.$$

The upper equation is then integrated as follows to obtain the vector form of resultant force of the normal force

$$\begin{cases} \overline{F_{N2}} = (F_{N2x}, F_{N2y}) \\ F_{N2x} = \int_0^{\theta_C} q_{N2x} d\theta = T_{holdt} \frac{1}{1+\mu^2} [(\sin \theta_C + \mu \cos \theta_C) \exp(\mu \theta_C) - \mu] \\ F_{N2y} = \int_0^{\theta_C} q_{N2y} d\theta = T_{holdt} \frac{1}{1+\mu^2} [(\mu \sin \theta_C - \cos \theta_C) \exp(\mu \theta_C) + 1] \end{cases}.$$

The magnitude of normal resultant force is

$$F_{N2} = \sqrt{F_{N2x}^2 + F_{N2y}^2} = T_{holdt} \sqrt{\frac{(\exp(\mu \theta_C) - \cos \theta_C)^2 + (\sin \theta_C)^2}{1 + \mu^2}}.$$

Combining Eqs. (4) and (9), the function expression of F_{N2} for the wrapping angle θ_C is

$$F_{N2} = T_0 \frac{\exp(-\mu \theta_C)}{1 - \mu_c \theta_C} \sqrt{\frac{(\exp(\mu \theta_C) - \cos \theta_C)^2 + (\sin \theta_C)^2}{1 + \mu^2}}.$$

As shown in Fig. 14, F_{N2} varies with the wrapping angle θ_C under different COFs in the range of $\mu \in [0.01, 0.6]$. The overall trend of F_{N2} is to grow slowly in the initial large range (0,80) and then grow rapidly in the final smaller range (80, $\theta_C(t_{end})$). F_{N2} is proportional to T_{holdt} , so there is also

a singularity of \tilde{L}^{-1} when the wrapping angle θ_C is close to $\theta_C(t_{end})$. In the same way, the actual end angle $\theta_C(t'_{end})$ can be considered to eliminate this singularity.

The comparison shown in Fig. 14f shows that, there is always a peak of F_{N2} in the first turn ($0, 2\pi$) of wrapping, and the magnitude of the peak decreases with the increase of the COF. However, the order of magnitude of F_{N2} is not greatly affected by the COF overall. In addition, when $\mu = 0.01$ as shown in Fig. 14a, F_{N2} exhibits a period-like oscillation behavior with an oscillation period of 2π , i.e. a turn of wrapping. When the COF is in the range of $\mu \in (0.1, 0.6)$ as shown in Fig. 14b–e, the amplitude of oscillation decays rapidly with the increase of wrapping angle, and the greater the COF, the faster the decaying.

Define that

$$f(\theta_C) = \frac{F_{N2x}}{F_{N2}} = \frac{[(\sin \theta_C + \mu \cos \theta_C)\exp(\mu\theta_C) - \mu]}{\sqrt{(1 + \mu^2)[(\exp(\mu\theta_C) - \cos \theta_C)^2 + (\sin \theta_C)^2]}}$$

θ_{C1} is the first wrapping angle that makes the equation $f(\theta_{C1}) = -1$ true, and θ_{C2} is the second wrapping angle after 0 that makes the equation $f(\theta_{C2}) = 1$ true. Then the direction of $\overline{F_{N2}}$ can be expressed as the azimuth angle

Table 1 Values of θ_{C1} and θ_{C2} for different COFs in Fig. 15

μ	θ_{C1} (rad)	θ_{C2} (rad)
0.01	5.931	6.635
0.1	5.242	7.251
0.2	4.892	7.433
0.3	4.660	7.459
0.6	4.240	7.303

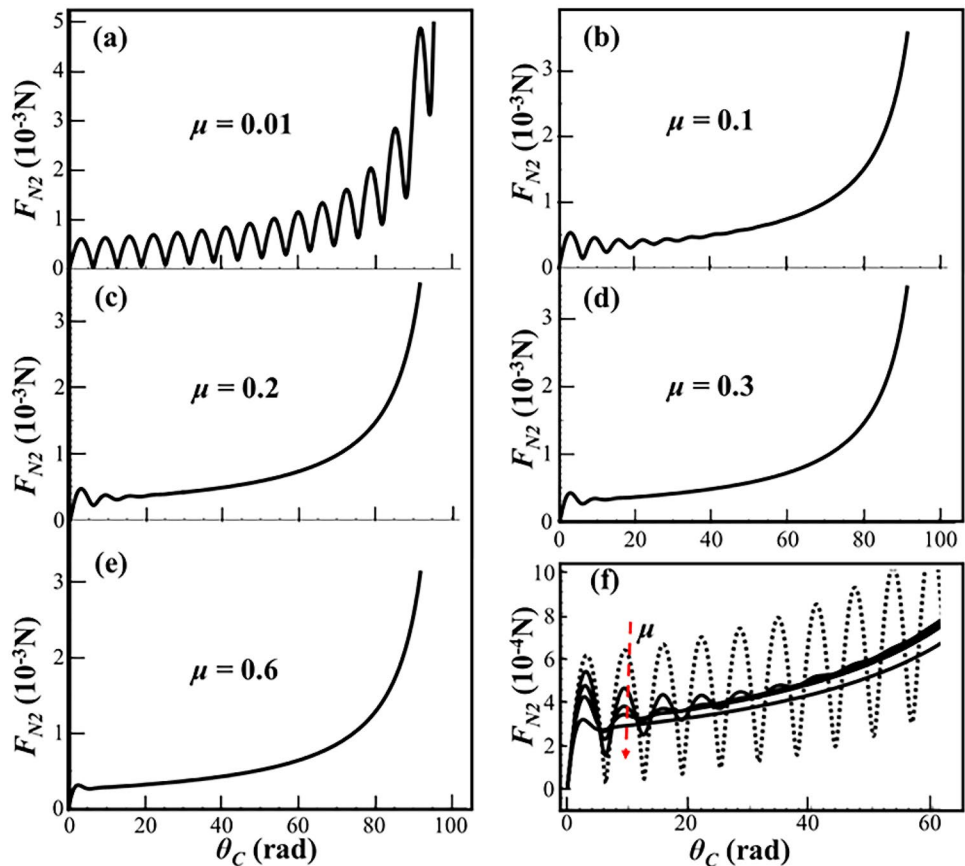
$$\alpha_{N2} = \begin{cases} \arccos(f(\theta_C)), & 0 \leq \theta_C \leq \theta_{C1} \\ 2\pi - \arccos(f(\theta_C)), & \theta_{C1} < \theta_C \leq \theta_{C2} \end{cases}$$

The subsequent change of α_{N2} repeats the feature in the range $(0, \theta_{C2})$ periodically.

As shown in Fig. 15, Tables 1 and 2, the azimuth angle α_{N2} of $\overline{F_{N2}}$ acting on the target object changes with the wrapping angle in the range of $(0, \theta_{C2})$. in the first turn of wrapping. It can be seen that within the first turn of wrapping ($\theta_C \in (0, 2\pi)$), α_{N2} increases with the increase of the COF at the same wrapping angle.

As shown in Fig. 16, arrows indicate the directions of force $\overline{F_{N2}}$, and the corresponding arcs indicate the wrapping ranges of rope. It can be seen that when the COF is small ($\mu = 0.01$), the azimuth angle α_{N2} has a good linear relationship with the wrapping angle θ_C as $\alpha_{N2} \approx \theta_{C2}/2$ in the range

Fig. 14 The magnitude F_{N2} of resultant force of the normal force acting on the target object varies with the wrapping angle under different COFs. $r_B = 0.1$ m, $v = 1$ m/s, $L_0 = 10$ m, $m_p = 0.003$ kg, $\mu_C = 0.01$. The COFs are (a) $\mu = 0.01$, (b) $\mu = 0.1$, (c) $\mu = 0.2$, (d) $\mu = 0.3$, (e) $\mu = 0.6$. (f) is the comparison of five curves in (a–e), and the red arrow indicates the direction of COF increase



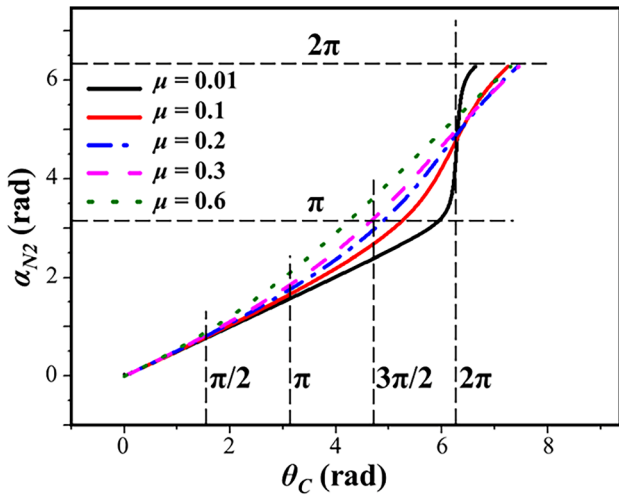


Fig. 15 The azimuth angle α_{N2} of $\overline{F_{N2}}$ varies with the wrapping angle θ_C under different COFs within the scope of $\theta_C \in (0, \theta_{C2})$. The parameter values are consistent with Fig. 14

of $\in \theta_C(0, 3\pi/2)$. This is because that the distribution of normal force $\overline{q_{N2}}$ is more uniform. However, the amplitude of change of α_{N2} is larger in the range of $\theta_C \in (3\pi/2, 2\pi)$, which is almost equivalent to that in the range of $\theta_C \in (0, 3\pi/2)$.

Combined with curves in Fig. 15, it is found that the greater the COF, the more the curve tends to be a straight line in the entire range of $\theta_C \in (0, \theta_{C2})$. This is because that the distribution of normal force $\overline{q_{N2}}$ is more uneven under the condition of large friction force.

Design of Preliminary Capture

Based on the mechanical analysis of wrapping process, it is possible to design a scheme for the initial capture in space using wrapping of rope. Initial capture, which is based on a satellite or space station, establishes a preliminary connection with a distant target by some means. The targets here can be non-cooperative space debris, asteroids, etc., or other cooperative satellites, space stations, etc. As a means

Table 2 Values of azimuth angle α_{N2} corresponding to wrapping angles $\pi/2, \pi, 3\pi/2$ and 2π under different COFs in Fig. 15

	θ_C			
	$\pi/2$	π	$3\pi/2$	2π
$\mu=0.01$	0.787544	1.5808	2.38975	4.72239
$\mu=0.1$	0.806848	1.67046	2.68322	4.81206
$\mu=0.2$	0.828236	1.76819	2.96743	4.90978
$\mu=0.3$	0.849501	1.86225	3.19445	5.00385
$\mu=0.6$	0.911981	2.11122	3.62292	5.25281

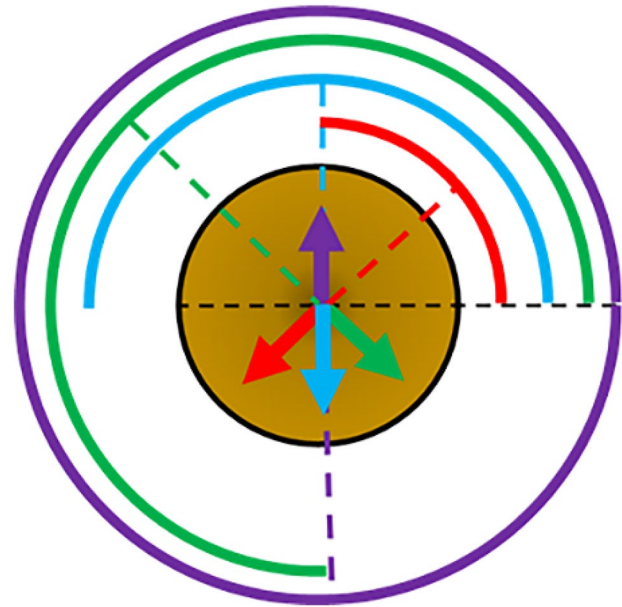


Fig. 16 Orientations of $\overline{F_{N2}}$ plotted from the data in Table 2. The red, blue, green and purple arrows represent the direction of force $\overline{F_{N2}}$ acting on the target object when the wrapping angles are $\pi/2, \pi, 3\pi/2$ and 2π respectively. And the red, blue, green and purple arcs are the wrapping situations of rope correspondingly. $\mu=0.01$

of space manipulation, the initial capture is a preparatory operation which facilitates the smooth progress of subsequent operations such as deorbiting space debris and precise docking with other spacecrafts.

According to the Euler-Eytelwein equation, when rope is at the edge of the sliding after the wrapping ends, there is the following relationship

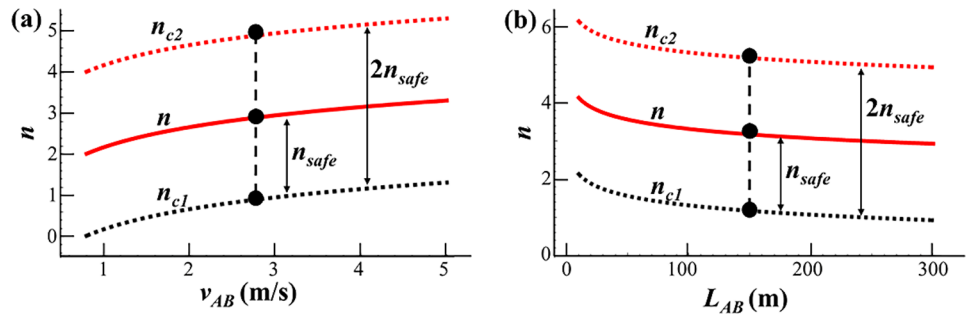
$$T_{loadp} = T_{holdp} \exp(\mu \theta_{end}) \tag{10}$$

where, T_{loadp} is the critical tension of the rope between the satellite and target, T_{holdp} is the support force of rope provided by the projectile on the other side of rope. The total angle that rope wraps at the end of the wrapping is

$$\theta_{end} = \frac{L_0}{r_B} = 2\pi n. \tag{11}$$

Without losing its generality, following capture situation is assumed: the direction of movement of target is consistent with the longitudinal direction of target, and the rope of segment L_{AB} is perpendicular to the longitudinal direction of target. In the initial period of time after wrapping ends, target B remains moving at a velocity v_{AB} relative to satellite A, and the two forms a new system of momentum exchange via a tether. The motion of the new system is characterized by overall translation while two bodies A and B rotate around certain centers. Due to the

Fig. 17 The design schemes of the number of wrapping turns using (a) v_{AB} and (b) L_{AB} to represent the information of target object, respectively. $r_B = 0.1$ m, $L_B = 1$ m, $\mu = 0.45$, $T_{holdp} = 0.3$ N, $m_{AB} = 50$ kg, $n_{safe} = 2$. $L_{AB} = 100$ m in (a) and $v_{AB} = 5$ m/s in (b)



difference of velocity between the satellite and target, the section L_{AB} of rope is tightened with the tension T_{AB} which causes the satellite and target one to slow down and the other to accelerate. For the sake of convenience, we estimate the expression of post-wrapping tension by dimensional analysis as

$$T_{loadp} = T_{AB} = m_{AB} \frac{v_{AB}^2}{L_{AB}}, \tag{12}$$

where, m_{AB} is a function of m_A and m_B with a dimension of mass, which we consider as $m_{AB} = \begin{cases} m_B, m_A \geq m_B \\ m_A, m_A < m_B \end{cases}$.

Solving simultaneous Eqs. (10)–(12), the constraint on the number of wrapping turns at the aspect of force (rope does not slide after the wrapping ends) is

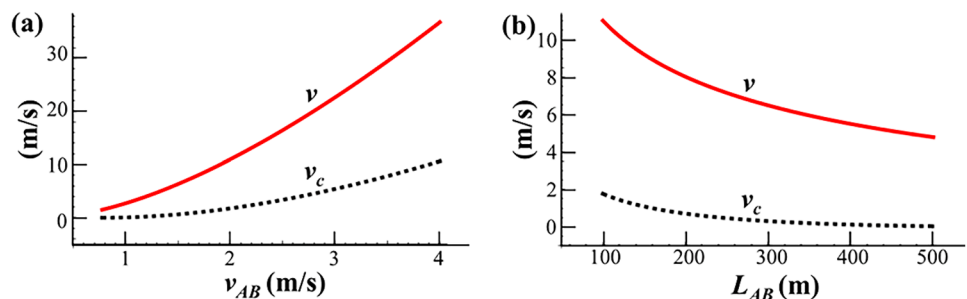
$$\begin{cases} n_{c1} = \frac{1}{2\pi\mu} \ln\left(\frac{m_{AB}v_{AB}^2}{T_{holdp}L_{AB}}\right) \\ n \geq n_{c1} \end{cases} \tag{13}$$

In addition, the time to finish the wrapping needs to be less than the time it takes for the target to pass through its own longitudinal length, that is, $t_{end} \leq L_B/v_{AB}$. Combining with the Eq. (6), the constraint on the number of wrapping turns at the aspect of time is obtained as

$$\begin{cases} n_{c2} = \sqrt{\frac{vL_B}{2\pi^2r_Bv_{AB}}} \\ n \leq n_{c2} \end{cases} \tag{14}$$

From Eqs. (13) and (14), composite constraints on the number of wrapping turns are

Fig. 18 The design velocity and critical velocity of projectile using (a) v_{AB} and (b) L_{AB} to represent the information of target object, respectively. $n_{safe} = 0.5$ and other parameter values are consistent with Fig. 17. $L_{AB} = 100$ m in (a) and $v_{AB} = 2$ m/s in (b)



$$\begin{cases} n_{c1} \leq n \leq n_{c2} \\ n_{c1} = \frac{1}{2\pi\mu} \ln\left(\frac{m_{AB}v_{AB}^2}{T_{holdp}L_{AB}}\right) \\ n_{c2} = \sqrt{\frac{vL_B}{2\pi^2r_Bv_{AB}}} \end{cases}$$

The constraint on the velocity of projectile is obtained from $n_{c1} \leq n_{c2}$ as

$$\begin{cases} v_c = \frac{2\pi^2r_Bv_{AB}n_{c1}^2}{L_B} \\ v \geq v_c \end{cases}$$

Figure 17 presents a design scheme for the number of wrapping turns. Consider an additional number of turns n_{safe} for safety, and the designed number of turns n is the mean of two critical values, i.e.

$$\begin{cases} n = \frac{(n_{c1} + n_{c2})}{2} \\ n_{safe} = \frac{(n_{c2} - n_{c1})}{2} \end{cases}$$

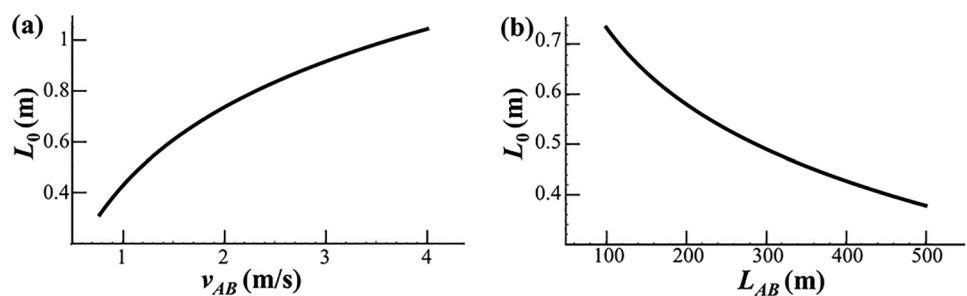
which results in

$$\begin{cases} n_{c2} = n_{c1} + 2n_{safe} \\ n = n_{c1} + n_{safe} \end{cases}$$

Combining the upper equations and Eqs. (2) and (5), designed values of the velocity of projectile and initial length of rope are got as

$$\begin{cases} v = \frac{2\pi^2r_Bv_{AB}}{L_B} (n_{c1} + 2n_{safe})^2 \\ L_0 = 2\pi r_B (n_{c1} + n_{safe}) \end{cases}$$

Fig. 19 Design values of initial rope length with (a) v_{AB} and (b) L_{AB} representing the information of target object, respectively. Parameter values are consistent with Fig. 18



of which visualized results are shown in Figs. 18 and 19.

In summary, the design procedure of preliminary capture is:

1. Observe or estimate material parameters (m_{AB}, μ) and geometric parameters (v_{AB}, L_{AB}, L_B, r_B) and calculate the critical number of wrapping turns n_{c1} .
2. Set the number of turns n_{safe} for safety, and calculate design parameters (v, L_0) of the tethered projectile system accordingly.

Summary and Discussion

In conclusion, the process that a tethered projectile system wraps around a target object in space is studied.

Through the decomposition and superposition of motion, characteristics of the WSM of projectile are analyzed when the rope wraps around a target object with circular cross-section are analyzed. The equations of motion for rope length, angular velocity, angle and trajectory are solved. The expression of total time is derived when wrapping around a target with regular N -sided cross-section, and consistent with the conclusion in the case of a circular cross-section when N tends to the limit of infinity. Displacements of projectile and wrapping times obtained by simulations of multibody dynamics are in good agreement with theoretical results.

Through force analysis, forces acting on the satellite under different COFs are obtained, and the extremum time and singularity are discussed. It is found that the greater the COF, the less the force on the satellite. And when the COF is large, it can be approximated that the force decreases with time, that is, the rope of section L_{AB} gradually relaxes. The vector form of resultant force of the normal force $\overline{F_{N2}}$ acting on the target object is obtained by the element force analysis. How the magnitude F_{N2} and azimuth angle α_{N2} change with the wrapping angle θ_C are compared under different COFs, and it is found that: (a) F_{N2} exhibits an oscillation behavior at the small COF, and the oscillation decays quickly when the COF is large; (b) There is a peak of F_{N2} in the first turn of wrapping which decreases with the increase of the COF; (c) α_{N2} increases with the increase of the COF within the first

turn of wrapping ($\theta_C \in (0, 2\pi)$); (d) α_{N2} is approximately half of θ_C in the range of $\theta_C \in (0, 3\pi/2)$ when the COF is small; (e) The greater the COF, the better the linear relationship between α_{N2} and θ_C in the entire range of $\theta_C \in (0, \theta_{C2})$.

There are two constraints at the aspects of force and time in the design of preliminary capture, and the number of wrapping turns needs to be between two critical number of turns. Taking into account the number of turns n_{safe} for safety, designed values of the number of wrapping turns n , the velocity of projectile v and initial length of rope L_0 are obtained. Finally, the design procedure of preliminary capture is proposed.

With regard to the future work, with reference to the existing casting schemes that considers gravity, it is possible to study the casting scheme in space that facilitates the subsequent realization of wrapping of a tethered projectile system.

Author Contribution Ding Lan designed the research ideas. Hongzhi Ma conducted the theoretical analysis and simulations and wrote the main manuscript text. Tao Wang and Fude Wang participated in the discussion. All authors reviewed the manuscript.

Funding This work is supported by the Strategic Priority Research Program of Chinese Academy of Sciences (Grant No. XDA17030100, Y820081XD1, Y820082XD1).

Data Availability The data collected during this study is available from the corresponding author upon reasonable request.

Declarations

Consent to Participate All authors consent to participate.

Consent for Publication All authors consent for publication.

Conflicts of Interest The authors declare that they have no conflict of interest.

References

Aglietti, G.S., Taylor, B., Fellowes, S., Salmon, T., Retat, I., Hall, A., Chabot, T., Pisseloup, A., Cox, C., Zarkesh, A., Mafficini, A., Vinkoff, N., Bashford, K., Bernal, C., Chaumette, F., Pollini, A., Steyn, W.H.: The active space debris removal mission RemoveDebris. Part 2: In orbit operations. *Acta Astronaut.* **168**, 310–322 (2020)

- Forshaw, J.L., Aglietti, G.S., Fellowes, S., Salmon, T., Retat, I., Hall, A., Chabot, T., Pisseloup, A., Tye, D., Bernal, C., Chaumette, F., Pollini, A., Steyn, W.H.: The active space debris removal mission RemoveDebris. Part 1: From concept to launch. *Acta Astronaut.* **168**, 293–309 (2020)
- Heath, T.L.: A history of Greek mathematics. Clarendon, Walton, UK (1921)
- Hill, L., Woodward, T., Arisumi, H., Hatton, R.L.: Wrapping a target with a tethered projectile. 2015 IEEE International Conference on Robotics and Automation (2015)
- Hill, L.P.: Ballistic rebounds for wrapping a target with a casting manipulator. Master of Science, Oregon State University (2018)
- Inaba, N., Oda, M., Asano, M.: Rescuing a stranded satellite in space - experimental robotic capture of non-cooperative satellites. *Trans. Jpn. Soc. Aeronaut. Space Sci.* **48**, 213–220 (2006)
- Ito, K., Yamakawa, Y., Ishikawa, M.: Winding manipulator based on high-speed visual feedback control. 2017-IEEE Conference on Control Technology and Applications (2017)
- Liu, Y.Q., Pan, D., Liu, Y.J., Tan, C.L.: Dynamics and capture strategy study of space rope-based end effectors. *Processing of 2014 International Conference on Multisensor Fusion and Information Integration for Intelligent Systems* (2014)
- Pan, D., Li, G.P., Zhang, H.B., Dai, S.J.: Dynamics investigate on capture process of rope end mechanism of space manipulator. 8th Symposium on Mechanics of Slender Structures (2020)
- Quadrelli, M.B., Ono, M., Jain, A.: Modeling of active tether system concepts for planetary exploration. *Acta Astronaut.* **138**, 512–529 (2017)
- Shan, M.H., Guo, J., Gill, E.: Review and comparison of active space debris capturing and removal methods. *Prog. Aerosp. Sci.* **80**, 18–32 (2016)
- Shi, X., Pan, Y.L., Ma, X.L.: Modeling and analysis of the rope-sheave interaction at traction interface. *J. Appl. Mech.* **84**(3), 031005 (2017)
- Sun, C., Wan, W.Y., Deng, L.S.: Adaptive space debris capture approach based on origami principle. *Int. J. Adv. Robot. Syst.* **16**(6), 1729881419885219 (2019)
- Suzuki, T., Ebihara, Y., Shintani, K.: Dynamic analysis of casting and winding with hyper-flexible manipulator. 2005 12th International Conference on Advanced Robotics (2005)
- Suzuki, T., Ebihara, Y., Suzuki, T., Ando, Y., Mizukawa, M.: Casting and winding manipulation with hyper-flexible manipulator. 2006 IEEE/RSJ International Conference on Intelligent Robots and Systems (2006)
- Xu, W.F., Yan, L., Hu, Z.H., Liang, B.: Area-oriented coordinated trajectory planning of dual-arm space robot for capturing a tumbling target. *Chin. J. Aeronaut.* **32**, 2151–2163 (2019)
- Xu, B.T., Yang, Y.N., Zhang, B., Yan, Y.: Simulation of space flexible webs on capture process based on nonlinear finite element method. 2019 5th International Conference on Mechanical and Aeronautical Engineering (ICMAE 2019) (2020)

Publisher's Note Springer Nature remains neutral with regard to jurisdictional claims in published maps and institutional affiliations.

Springer Nature or its licensor (e.g. a society or other partner) holds exclusive rights to this article under a publishing agreement with the author(s) or other rightsholder(s); author self-archiving of the accepted manuscript version of this article is solely governed by the terms of such publishing agreement and applicable law.